Biopolymers

WILEY

Biopolymers

ARTICLE

Synthesis and Investigation of Albumin Nanoparticles Loaded With Anti-Tuberculosis Drug Isoniazid

Aldana Galiyeva[1] | Yerkeblan Tazhbayev[1] | Tolkyn Zhumagaliyeva[1] | Bakhytgul Karimova[1] | Nurlan Tabriz[2] | Vitaliy V. Khutoryanskiy[3]

[1]Department of Organic Chemistry and Polymers, Buketov Karaganda University, Karaganda, Kazakhstan | [2]Department of Infectious Diseases and Phthisiolog, Karaganda Medical University, Karaganda, Kazakhstan | [3]Reading School of Pharmacy, University of Reading, Reading, UK

Correspondence: Aldana Galiyeva (aldana_karaganda@mail.ru) | Yerkeblan Tazhbayev (e.tazhbayev@gmail.com)

Received: 6 February 2025 | **Revised:** 26 May 2025 | **Accepted:** 30 May 2025

Funding: This work was supported by the Science Committee of the Ministry of Science and Higher Education of the Republic of Kazakhstan (Grant AP25794971) "Creation of PEGylated polymer nanosystems immobilized with anti-tuberculosis drug substances for the treatment of tuberculosis" and (Grant AP14871344) "Development of colloidal biopolymer-based drug delivery systems for tuberculosis chemotherapy." V.V.K. acknowledges the Royal Society for his industry fellowship (IF\R2\222031).

Keywords: albumin | cysteine | isoniazid | nanoparticles | urea

ABSTRACT

The development of novel treatment strategies for tuberculosis (TB), including its multidrug-resistant forms, remains a global health priority. Conventional first- and second-line anti-TB drugs are often incorporated into polymer-based delivery systems to improve efficacy and reduce side effects. Among biodegradable, non-toxic, and biocompatible polymers, human serum albumin (HSA) stands out as a highly promising drug carrier. In this study, isoniazid (INH)-loaded human serum albumin nanoparticles were synthesized via the reaction of HSA macromolecules with cysteine in the presence of urea. Key nanoparticles characteristics—including size, polydispersity, drug loading efficiency, and drug binding capacity—were systematically evaluated and optimized. The effects of various formulation parameters, such as solution pH and concentration of urea, cysteine, albumin, and isoniazid, were investigated. Conformational changes in the protein structure were assessed using spectrofluorometric analysis. Additionally, the physicochemical properties and in vitro drug release profiles of HSA-INH nanoparticles were characterized. The antimicrobial activity of the nanoparticles was tested against the wild-type *Mycobacterium tuberculosis* H37Rv strain at isoniazid concentrations of 5, 25, and 50 mg/mL. The minimum inhibitory concentration of isoniazid when delivered via HSA nanoparticles was also determined.

1 | Introduction

Tuberculosis remains one of the most significant global health threats, being the leading cause of death from infectious diseases and ahead of diseases such as HIV/AIDS and COVID-19 [1]. *Mycobacterium tuberculosis* (MTB) is the bacterium responsible for causing this condition. The pathogen usually affects the lungs, but it can also affect other parts of the body. The disease is spread in the air from tuberculosis patients, for example, via coughing [2]. According to the World Health Organization, about a quarter of the world's population is at risk of developing tuberculosis. The disease moves into the active stage with a decrease in immunity, so the likelihood of the disease is high in patients with human immunodeficiency virus, diabetes, and other chronic conditions [3, 4]. Despite great efforts in all countries, the epidemiological situation with TB is difficult to control. About 10.8 million people get infected with tuberculosis every year worldwide, and the incidence of TB has recently remained at a relatively stable level. In 2023, the number of deaths from tuberculosis is estimated

at 1.25 million people [1]. This situation is further complicated by the fact that over half a million cases of multiple drug-resistant tuberculosis are identified each year, with fewer than 68% ultimately cured [1]. Traditional TB therapy is not only insufficiently effective but also disrupts the structural and functional integrity of lung tissue (morpho-functional imbalance), increases systemic toxicity, and contributes to the development of drug resistance [5, 6].

TB therapy usually includes several medications that must be taken for 6 months and can even be extended for up to 12 months. The US Food and Drug Administration has so far approved ten drugs for tuberculosis treatment [7]. Isoniazid (INH) is a widely available and cost-effective drug commonly used in the chemotherapy of tuberculosis caused by MTB. INH exhibits strong bacteriostatic activity against various forms and localizations of MTB [8, 9]. Although isoniazid has good pharmacokinetic and pharmacodynamic properties, its efficacy is highly dependent on regular administration. Disruption of the treatment regimen may lead to the development of drug resistance. Isoniazid is also rapidly excreted from the body, necessitating the use of high doses that can cause toxic effects. Furthermore, a large proportion of the administered drug undergoes biotransformation before exerting its antibacterial effect. Developing an effective drug carrier that ensures sustained release, targeted delivery, and prevention of drug resistance is a promising strategy to improve treatment outcomes. Encapsulation of isoniazid in nanoparticles enables controlled drug release, maintains stable levels, and facilitates direct delivery to the target cells, thereby enhancing treatment efficacy and reducing the risk of side effects [10, 11].

Biopolymers, particularly serum albumin, are promising drug carriers due to their natural role in transporting biologically active substances in the body. The presence of numerous amino-, carboxyl, amide, and other functional groups in albumin's primary structure, along with specific binding sites, makes it an ideal candidate for developing bioconjugates with various pharmacologically active compounds [12, 13]. Preparation of HSA nanoparticles as potential drug carriers is of substantial interest. Glutaraldehyde is commonly used to stabilize protein nanoparticles prepared by desolvation [14–17]. The primary drawback of glutaraldehyde usage is its cytotoxicity, which can trigger adverse biological reactions, including inflammation and immune responses [18, 19]. Additionally, the extensive cross-linking induced by glutaraldehyde treatment can cause undesirable structural modifications in proteins, potentially impairing both drug delivery and release properties [20, 21]. In recent years, research into alternative, less toxic crosslinking agents derived from natural compounds has gained considerable attention. Previous studies have demonstrated the successful preparation of stable HSA nanoparticles through the interaction of the protein with cysteine in the presence of urea, including their loading with anticancer drugs [22, 23]. However, the application of biocompatible components for creating HSA nanoparticles to deliver anti-TB drugs remains poorly explored.

In the present study, the feasibility of preparing HSA nanoparticles using biocompatible components and loading them with isoniazid was investigated for the first time. The novelty of this study lies in the comprehensive analysis of key factors influencing nanoparticle formation, stability, and properties, including the concentrations of HSA, L-cysteine, urea, and isoniazid, as well as environmental conditions such as pH. Additionally, the release profile of isoniazid from the nanoparticles was examined, and the minimum inhibitory concentration of isoniazid-loaded HSA nanoparticles required to inhibit the growth of *Mycobacterium tuberculosis* was determined.

2 | Materials and Methods

2.1 | Materials

HSA (lyophilized powder, 98% purity), isoniazid (≥ 99% purity) and L-cysteine (98.5% purity) were purchased from Sigma-Aldrich (Germany). Absolute ethanol was purchased from DosFarm (Almaty, Kazakhstan). Urea (99.5% purity) was purchased from HimPribor-SPb (Saint Petersburg, Russia).

2.2 | Preparation of HSA NPs

HSA-derived nanoparticles (NPs) were produced by the desolvation method in accordance with a slightly modified procedure described elsewhere [22–24]. In brief, the pre-set amount of serum albumin powder was dissolved in 3 mL of distilled water by stirring at 200 rpm at 23°C for 10 min (the concentrations of these protein solutions were 10, 20, 40, and 80 mg/mL). The solution pH was adjusted to 4–9 with 0.5 mol/L HCl and NaOH. Thereupon, 16 mL of ethanol was added to each protein solution at a rate of 1 mL/min, thus resulting in a turbid dispersion of albumin nanoparticles. Then, 0.5 mL of aqueous solutions of urea at 1, 2, 3, 4, 5, 6, 7, and 8 mol/L was added to each protein solution, followed by the introduction of 3 mL of aqueous 1, or 2.5, or 5, or 10 mg/mL L-cysteine solution. Every reaction mixture prepared in this way was stirred continuously for 2 h. Exactly 3 mL of isoniazid solution was added to the reaction mixture so that the concentrations of the drug in the system were 2, 4, 6, and 8 mg/mL. The drug loading was conducted under constant magnetic stirring at 300 rpm for 2 h. The resultant suspension of nanoparticles was washed with distilled water and isolated using three centrifugation steps (MiniSpi, Eppendorf, Hamburg, Germany) at 14,000 rpm for 15 min each to remove dissolved substances and ethanol from the mixture. The precipitated nanoparticles were re-dispersed in 10 mL of distilled water after each phase of centrifugation using an ultrasonic bath (Launch Tech, Shenzhen, China); the ultrasound treatment time was 10 min.

2.3 | Nanoparticles Size Measurement, Zeta Potential Analysis, and Surface Morphology

The average particle size, polydispersity index (PDI) and zeta potential of the HSA-NPs, both with and without isoniazid, were measured using dynamic light scattering (DLS) with Zetasizer NanoZS90 (Malvern Instruments Limited, Worcestershire, UK). The samples were diluted with deionized water and measured at a scattering angle of 90° at 25°C. The isoelectric points of drug-free and isoniazid-modified HSA nanoparticles were determined using electrophoretic mobility measurements while varying the

pH of solutions [25]. Size, shape, and surface morphology of the HSA-NPs were examined using scanning electron microscopy (SEM, MIRA 3LM TESCAN, Brno, Czech Republic, EU). For SEM spectroscopy, dried nanoparticles were mounted onto a sample holder and coated with carbon. Carbon-coated conductive adhesive tapes were used to adhere the samples to the sample holders. The SEM images were analyzed using ImageJ software.

2.4 | Encapsulation Efficiency, Drug Loading, and Production Yield

After centrifugation and washing of the nanoparticles, the supernatant was collected and the drug concentration in the solution was determined using high performance liquid chromatography (HPLC) method (Shimadzu LC-20 Prominence, Japan). The amount of drug encapsulated within the nanoparticles was calculated by subtracting the free (unencapsulated) drug present in the supernatant from the total drug amount. Encapsulation efficiency, drug loading, and production yield were calculated as follows:

$$\text{Encapsulation efficiency}\,(\%) = \frac{\text{Total mass of the Drug} - \text{Mass of free Drug}}{\text{Total mass of the Drug}} \times 100\%$$

$$\text{Drug loading}\,(\%) = \frac{\text{Total mass of the Drug} - \text{Mass of free Drug}}{\text{Total mass of nanoparticles}} \times 100\%$$

$$\text{NPs yield}\,(\%) = \frac{\text{Total mass of nanoparticles}}{\text{Total mass of the Drug} + \text{Total mass of HSA}} \times 100\%$$

2.5 | In Vitro Drug Release

For drug release experiments, 24 mg of nanoparticles were redispersed in 14 mL of phosphate-buffered saline (PBS, pH 7.4) and incubated at 37°C with stirring at 200 rpm. At different time intervals (0, 2, 4, 8, 12, and 24 h), 1 mL aliquots were withdrawn, centrifuged, and the supernatant containing the released drug was analyzed using HPLC at 262 nm. All measurements were performed in triplicates. The cumulative drug release was plotted as a function of time.

2.6 | Fluorescence Measurements

Exactly 5 mL HSA solutions (0.66 g/L) prepared in distilled water were used to record their fluorescence spectra. The solution pH was adjusted to 4–9 with 0.5 mol/L HCl and NaOH. Urea was dissolved in the protein solution to reach the concentrations of 1–10 mol/L. L-cysteine was dissolved in the protein solution to make the solutions with the concentrations of 1, 2.5, 5, and 10 mg/mL. Intrinsic fluorescence values were measured using a Cary Eclipse fluorescent spectrophotometer (Agilent Technologies). The excitation wavelengths for measuring intrinsic fluorescence values were 280 and 295 nm; almost all the excitation energy is absorbed by protein tryptophanyl residues at 295 nm. The fluorescence spectra were recorded in the wavelength range from 300 to 650 nm. The width of the emission and absorption slits in the measurement of intrinsic fluorescence was taken as 5 nm. A pulsed xenon lamp was used as the excitation source.

2.7 | Thermal and Spectroscopic Characterization of the Nanoparticles

Thermogravimetric (TGA) and differential scanning calorimetry (DSC) analysis were performed on a LabSYS evo TGA/DTA/DSC analyzer (Setaram, France) in the temperature range of 30°C–550°C in an aluminum oxide crucible at a heating rate of 10°C/min in a nitrogen atmosphere (30 mL/min).

FTIR spectra of the nanoparticles were recorded using IR spectroscopy (FSM 1202 LLC "Infraspect," Russia). A total of 3 mg of each sample was mixed with 100 mg of KBr, and a pellet was prepared using a KBr tablet press.

2.8 | In Vitro Study of the Inhibitory Activity of HSA Nanoparticles Loaded With Isoniazid

In vitro experiments were conducted using Airstream AC2-4E8 biosafety cabinets (Esco Micro Pte. Ltd., Singapore), which ensured sterile working conditions by maintaining negative air pressure and filtering air through HEPA filters. The antimycobacterial activity of the nanoparticles was studied using an antituberculosis drug-sensitive wild strain of MTB H37Rv obtained from the pulmonary clinic Asklepios (Munich-Gauting, Germany). The in vitro bacteriostatic activity of the nanoparticles was assessed by evaluating the growth of the MTB strain in Levenstein–Jensen nutrient-dense medium. The test tubes with inoculations were incubated for 4 weeks, after which the results were recorded. The results of the suppressive activity were evaluated by counting the number of colony forming units (CFU) of MTB on nutrient-dense medium and comparing the control and experimental cultures. Bacterial samples with positive detections were further processed using the Ziehl–Neelsen staining method according to Dzodanu et al. [26]. The dried smears were then examined under a Leica DMLS microscope.

2.9 | Statistical Analysis

The data are expressed as mean ± standard deviation, and statistical analysis was carried out using Minitab 19 Statistical Software. One-way analysis of variance (ANOVA) was used to evaluate the statistical significance of the results.

3 | Results and Discussion

3.1 | Optimization of Nanoparticles Preparation

3.1.1 | Preparation of HSA-INH NPs Using the Previously Developed Method

Nanoparticles of human serum albumin loaded with isoniazid were prepared in the presence of L-cysteine and urea using the method previously reported for the synthesis of nanoparticles loaded with hydroxyurea [22, 23]. This work study aimed to modify the previously reported method by replacing the conventional crosslinking agent (glutaraldehyde) with a combination of urea and L-cysteine. Urea affects the conformation

of serum albumin, causing partial unfolding of its globular structure with the exposure of hydrophobic amino acid groups to the surface. L-cysteine then reacts to break intramolecular disulfide bonds in protein macromolecules, leading to a better unfolding of the polypeptide chains [23]. Consequently, covalent intermacromolecular S-S bonds are formed as a result of the thiol-disulfide exchange reaction [22, 27–30]. In addition, hydrophobic interactions and, to a lesser extent, newly formed hydrogen and ionic bonds play a significant role in stabilizing the spatial structure of polymer nanoparticles. Therefore, the yield of HSA nanoparticles prepared via ethanol-induced desolvation followed by stabilization with urea and L-cysteine exceeded 50%. Both the encapsulation efficiency of isoniazid and its incorporation into the polymer matrix were high. However, the particle size of the resulting HSA-INH nanoparticles was 394 ± 9 nm, which exceeds the desired optimal range of 50–300 nm [31] (Table 1).

Considering the presence of many reactive functional groups in HSA structure, it can be assumed that changing the synthesis conditions will affect the characteristics of the final product. There are several possible parameters for optimization of the synthesis conditions, including the solution pH, the concentration of reacting components, and drugs.

3.1.2 | Effect of HSA Solution pH

Solutions of HSA and HSA-INH were prepared at pH values ranging from 4 to 9, followed by the addition of an equal volume of ethanol to each. After desolvation, the resulting protein solutions exhibited distinct visual appearances (Figure S1).

It is well known that albumins undergo reversible conformational transitions upon changes in solution pH [32]. This can certainly affect the subsequent stages of the NPs synthesis, their characteristics, and the yield of the final product. Fluorescence spectroscopy is an informative method to study the transitions in proteins [32]. It is known that HSA consists of a single long polypeptide chain with 586 amino acids, packed into 3 linked globular segments; the conformation of which is fixed by 17 disulfide bonds [33–35]. The intrinsic fluorescence of HSA is mainly due to a single Trp-214 residue in the hydrophobic cavity of subdomain IIA (Sudlow I). Previously, Dockal et al. investigated tyrosyl fluorescence to obtain additional insights into the structural characteristics of proteins [36]. Figure 1 shows the fluorescence emission spectra of HSA nanoparticles in solutions prepared at different pHs upon excitation at 280 nm. The fluorescence intensity of HSA depends on the solution pH (Figure 1). It is known that the protein takes the native form at a pH value close to 7.0 [33]. An increase in fluorescence intensity at pH values above and below 7.0 may be attributed to the emergence of uncompensated positive and negative charges on the surface of biopolymer macromolecules, resulting from the dissociation of amino acid side chains. This charge imbalance promotes repulsion between like-charged functional groups, leading to the partial unfolding of HSA macromolecules into their F and B conformational forms.

As the pH of the HSA solution decreases from pH 6.0 to pH 4.0, the fluorescence intensity of tyrosine diminishes, accompanied by a slight blue shift in the emission maximum from 336 to 333 nm. This change is likely due to proton redistribution around the aromatic ring mediated by nearby carboxyl groups [33]. In the pH range from 6.0 to 9.0, tyrosine fluorescence intensity also decreases, while the emission maximum exhibits a slight but reproducible red shift from ~336 to ~339 nm. These observations are consistent with findings reported by Dockal et al. [36].

Following desolvation of protein macromolecules with ethanol, urea and L-cysteine were added sequentially to the solution. The mechanism of the protein reactions with urea and L-cysteine is described in detail in [37]. Table 2 shows the characteristics of the prepared nanoparticles. The nanoparticles with substantial yield were prepared in the pH range from

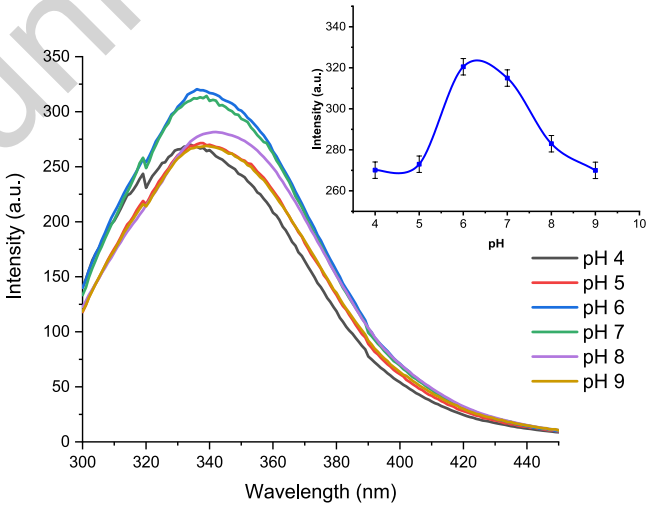

FIGURE 1 | Fluorescence spectra of HSA nanoparticles recorded in solutions with different pHs. Insert: pH dependence of the intensity of the tyrosine fluorescence maximum in solution upon excitation at 280 nm (Figure S2).

TABLE 1 | Characteristics of Nanoparticles and Production Efficiency (pH 7.4, HSA concentration—20 mg/mL, L-cysteine concentration—1 mg/mL).

	Characteristics of nanoparticles				Production efficiency	
NPs	Size (nm)	PDI	Zeta potential (mV)	Encapsulation efficiency (%)	Drug loading (%)	NPs yield (%)
HSA	244 ± 7	0.317 ± 0.021	−14 ± 3	—	—	69 ± 5
HSA-INH	394 ± 9	0.232 ± 0.067	−21 ± 3	85 ± 2	15 ± 2	56 ± 5

Note: All values are presented as the mean ± SD ($n = 3$).

TABLE 2 | Characteristics of nanoparticles and production efficiency using different pH.

		Characteristics			Production efficiency		
NPs	pH	Size (nm)	PDI	Zeta potential (mV)	Encapsulation efficiency (%)	Drug loading (%)	NPs yield (%)
HSA	4	144 ± 6	0.207 ± 0.064	−5 ± 2	—	—	3 ± 1
	5	169 ± 8	0.427 ± 0.058	−19 ± 2	—	—	78 ± 4
	6	216 ± 13	0.378 ± 0.047	−31 ± 4	—	—	63 ± 5
	7	244 ± 7	0.317 ± 0.021	−14 ± 3	—	—	69 ± 6
	8	71 ± 8	0.317 ± 0.079	−22 ± 3	—	—	18 ± 3
	9	60 ± 9	0.098 ± 0.023	−39 ± 4	—	—	2 ± 1
HSA-INH	4	146 ± 7	0.191 ± 0.025	−5 ± 2	75 ± 5	3 ± 3	2 ± 1
	5	175 ± 2	0.494 ± 0.057	−6 ± 5	73 ± 8	12 ± 3	53 ± 7
	6	211 ± 9	0.183 ± 0.021	−28 ± 1	78 ± 8	10 ± 3	68 ± 3
	7	394 ± 9	0.232 ± 0.067	−21 ± 3	85 ± 7	15 ± 4	56 ± 5
	8	88 ± 5	0.384 ± 0.049	−26 ± 3	81 ± 7	3 ± 1	2 ± 1
	9	71 ± 8	0.405 ± 0.060	−27 ± 4	92 ± 4	7 ± 4	1.0 ± 0.1

Note: All conditions, except pH, were consistent with the standard parameters. Data for pH 7 were taken from Table 1. All values are presented as mean ± SD ($n = 3$).

5 to 7, both for drug-free and INH-loaded nanoparticles. The particle size and polydispersity values observed within the pH range were also within acceptable limits. Above and below this pH range, the yield of nanoparticles was relatively low, which indicates that these conditions are not suitable for the synthesis of nanoparticles. At pH = 6 the values of zeta potential of HSA and HSA-INH nanoparticles are in the range of −28 to −31 mV, which indicates that these samples are colloidally stable. These observations are in good agreement with the study of Langer et al. [15]. As shown, both drug-free HSA and isoniazid-modified nanoparticles have an isoelectric point around pH 4. Below this value, most of the amino and carboxyl groups are in the protonated state, resulting in a positive surface charge of the nanoparticles. On the contrary, at pH above the isoelectric point, deprotonation of these functional groups occurs, which leads to the predominance of negative charge on the particle surface [38].

Further studies were aimed at elucidating the effects of urea concentration on the physicochemical characteristics of nanoparticles in terms of their particle size, polydispersity, and yield.

3.1.3 | Study of Urea Concentration Effect

Previous studies [22, 23] demonstrated that the use of a mild chaotropic agent is essential for enhancing the availability of HSA functional groups for thiol-disulfide exchange during nanoparticle synthesis. In this work, we have used urea as a chaotropic agent in the synthesis of nanoparticles. Urea binds reversibly to proteins, disrupting intermolecular hydrogen bonds regardless of its concentration in solution [39]. While some studies report that protein denaturation by urea is reversible [40, 41], others suggest it is not. In this work, interactions between urea and the protein were examined to identify the optimal urea concentration and the most effective method of its addition. This aims to ensure efficient unfolding of biomacromolecules involved in thiol-disulfide exchange reactions in the presence of cysteine.

As was discussed above, fluorescence spectroscopy can be used to probe the changes in the protein conformation. It is known that albumin fluorescence originates from tryptophan (Trp), tyrosine (Tyr), and phenylalanine residues [42]. Figure 2 shows the fluorescence spectra of the protein recorded at different concentrations of urea upon excitation at 280 and 295 nm, which excite tyrosine and tryptophan residues of HSA, respectively. Tyr fluorescence (280 nm) provides limited information on the changes in protein structure, as it has been shown in a number of studies to be almost completely quenched upon ionization of the amino group, of the carboxyl group of Trp [42, 43]. However, some changes in the conformation of protein biomacromolecules can still be observed (Figure 2a), which is associated with the changes in the neighborhood of tryptophan residues [33]. The intensity of Trp (Figure 2b) fluorescence decreases with increase in the concentration of urea; however, this effect is observed only at $C_{urea} > 2$ mol/L. It is known [33] that tyrosine fluorescence of albumin is an indicator of domain structure change upon protein denaturation. Some authors believe [43, 44] that tyrosine fluorescence is an indicator of changes in the primary hydration shell of biomacromolecules, which is associated with the redistribution of hydrogen bonds between surface amino acid groups and solvent molecules. Consequently, the observed changes in the intensity of the spectra with increasing urea concentration support the hypothesis that hydrogen bonds are responsible for protein denaturation in the presence of these chaotropic agents [45, 46].

At low urea concentrations (< 2 mol/L), there were practically no differences in the fluorescence intensity when

excited at 280 and 295 nm. A substantial reduction in the fluorescence intensity was observed in the concentration range of C_{urea} = 2–7 mol/L, which may be a result of the quenching of tryptophan fluorescence due to the denaturation of domains II and III [47]. In the concentration range of C_{urea} = 7–10 mol/L, the fluorescence intensity reaches a plateau with low values.

The results of the study of urea concentration effect on the characteristics of the nanoparticles formed in the absence and in the presence of isoniazid are presented in Table 3.

At a urea concentration of 4 mol/L, HSA nanoparticles with an average size of 287 ± 1 nm and low polydispersity (0.039 ± 0.06) were formed with a high yield (99%). Increasing the urea

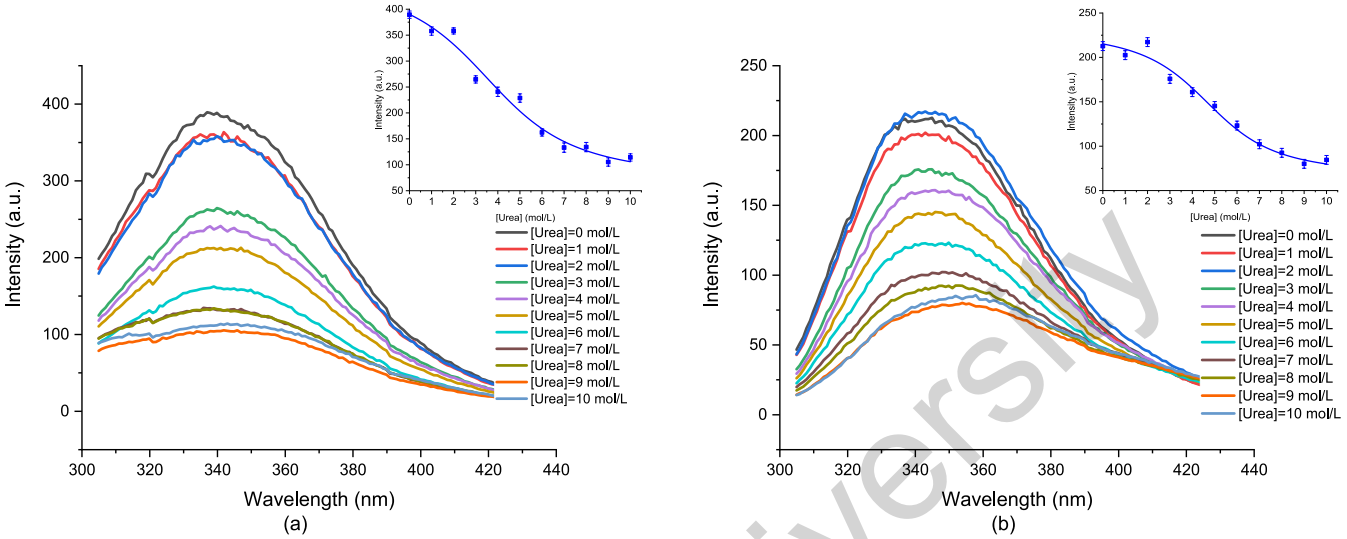

FIGURE 2 | Fluorescence spectra of HSA in the presence of urea recorded upon excitation at 280 nm (a) and 295 nm (b). Inserts show dependence of the fluorescence intensity of tyrosine and tryptophan residues of HSA on the concentration of urea (Figures S3 and S4).

TABLE 3 | Characteristics of nanoparticles prepared in solutions of urea.

NPs	Urea concentration (mol/L)	Characteristics			Production efficiency		
		Size (nm)	PDI	Zeta potential (mV)	Encapsulation efficiency (%)	Drug loading (%)	NPs yield (%)
HSA	1	245 ± 9	0.165 ± 0.049	−28 ± 1	—	—	68 ± 7
	2	301 ± 5	0.082 ± 0.011	−27 ± 3	—	—	62 ± 7
	3	269 ± 10	0.172 ± 0.127	−31 ± 4	—	—	71 ± 4
	4	287 ± 1	0.039 ± 0.061	−27 ± 2	—	—	98 ± 2
	5	407 ± 6	0.090 ± 0.023	−18 ± 1	—	—	75 ± 6
	6	296 ± 5	0.164 ± 0.039	−23 ± 7	—	—	58 ± 9
	7	158 ± 9	0.297 ± 0.018	−24 ± 3	—	—	14 ± 6
	8	106 ± 7	0.456 ± 0.055	−16 ± 3	—	—	13 ± 4
HSA-INH	1	264 ± 7	0.081 ± 0.098	−20 ± 5	75 ± 8	11 ± 3	60 ± 7
	2	277 ± 6	0.059 ± 0.072	−28 ± 3	80 ± 7	11 ± 4	56 ± 8
	3	241 ± 9	0.195 ± 0.030	−27 ± 2	80 ± 6	13 ± 5	56 ± 6
	4	217 ± 8	0.168 ± 0.032	−16 ± 1	80 ± 9	23 ± 5	31 ± 4
	5	254 ± 9	0.125 ± 0.041	−19 ± 6	85 ± 9	20 ± 6	38 ± 4
	6	281 ± 6	0.090 ± 0.033	−33 ± 3	85 ± 5	15 ± 4	53 ± 6
	7	148 ± 9	0.327 ± 0.046	−14 ± 2	46 ± 7	21 ± 4	20 ± 6
	8	160 ± 2	0.536 ± 0.022	−12 ± 1	63 ± 7	11 ± 2	13 ± 6

Note: All conditions, except urea concentration, were maintained to standard parameters. Data are presented as the mean ± SD (n = 3).

concentration to 7 and 8 mol/L resulted in the formation of smaller nanoparticles (106–158 nm), but with significantly lower yield. For the preparation of HSA-INH nanoparticles, the optimal urea concentration range was 4–6 mol/L, producing nanoparticles with diameters of 217–281 nm, polydispersity indices of 0.090–0.168, and yields ranging from 31% to 53%. Drug loading reached up to 23%.

3.1.4 | Effect of L-Cysteine Concentration

More efficient formation of nanoparticles was achieved using L-cysteine, which can cleave intramolecular disulfide bonds in proteins. This promotes more complete unfolding of the protein chain and facilitates the interaction of L-cysteine with intramolecular S–S bridges within the HSA globule [18]. The subsequent formation of intermolecular disulfide bonds by thiol-disulfide exchange represents a post-translational modification of the protein structure.

The characteristics of HSA and HSA-INH nanoparticles prepared at different concentrations of L-cysteine (1–10 mg/mL) are presented in Table 4. An improvement in all parameters both for drug-free formulations and for INH-loaded nanoparticles was observed with L-cysteine concentration of 5 mg/mL, resulting in nanoparticles of 97 ± 6 nm and 113 ± 5 nm, respectively. In the latter case, a particle size distribution was close to monomodal (PDI 0.08 ± 0.01). The yield of NPs and the drug loading were satisfactory. However, increasing the concentration of L-cysteine above 5 mg/mL negatively impacted all system parameters. This concentration likely represents the saturation point of terminal cysteine units, indicating the stabilization of HSA nanoparticles had been achieved through thiol disulfide exchange reactions.

Spectrofluorometric analysis revealed that increasing the L-cysteine concentration from 1 to 5 mg/mL enhances the excitation of the protein's chromophore groups (Figure 3), suggesting spatial modification in the albumin structure. This effect is likely due to the formation of S–S bridges within the HSA globule. At L-cysteine concentrations above 5 mg/mL, a decrease in fluorescence intensity is observed, indicating the potential reduction of newly formed interchain S–S bridges [12], which disrupts the intramolecular structuring necessary for stable protein nanoparticle formation.

3.1.5 | Effect of HSA Solution Concentration on the Properties of Nanoparticles

Biopolymer concentration is another factor influencing the properties of nanoparticles. Table 5 presents the characteristics of the HSA-NPs and HSA-INH-NPs prepared at various albumin concentrations.

The optimal concentration of the initial albumin to prepare HSA-NPs is 40 mg/mL. In this case, a high yield of HSA nanoparticles

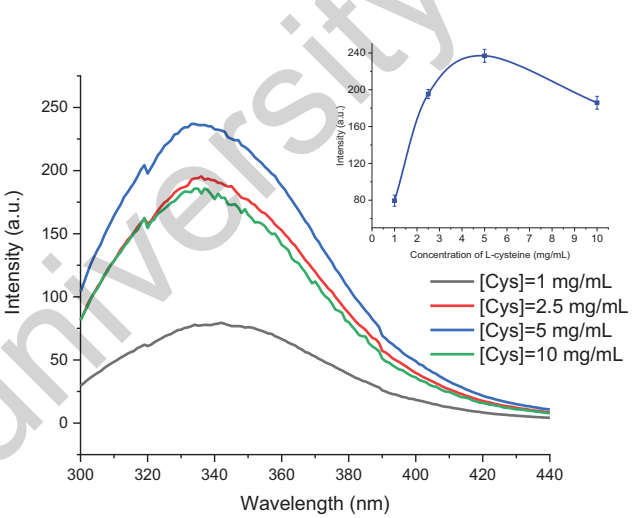

FIGURE 3 | Fluorescence spectra of HSA in the presence of L-cysteine recorded upon excitation at 280 nm. Insert shows the dependence of tyrosine fluorescence intensity on L-cysteine concentration (Figure S5).

TABLE 4 | Characteristics of nanoparticles and production efficiency using different L-cysteine concentrations.

Nano-particles	L-cysteine concentration (mg/mL)	Characteristics			Production efficiency		
		Size (nm)	PDI	Zeta potential (mV)	Encapsulation efficiency (%)	Drug loading (%)	NPs yield (%)
HSA	1	244 ± 7	0.317 ± 0.021	−14 ± 3	—	—	69 ± 6
	2.5	216 ± 5	0.154 ± 0.021	−42 ± 11	—	—	76 ± 6
	5	97 ± 6	0.209 ± 0.056	−36 ± 10	—	—	78 ± 5
	10	145 ± 8	0.075 ± 0.084	−42 ± 3	—	—	88 ± 4
HSA-INH	1	394 ± 9	0.232 ± 0.067	−21 ± 3	85 ± 6	7 ± 3	56 ± 7
	2.5	206 ± 5	0.121 ± 0.041	−36 ± 2	69 ± 4	9 ± 4	76 ± 3
	5	113 ± 5	0.083 ± 0.012	−31 ± 2	73 ± 5	15 ± 2	89 ± 9
	10	259 ± 10	0.118 ± 0.086	−50 ± 5	—	—	76 ± 7

Note: All conditions, except L-cysteine concentration, were maintained according to standard parameters. Data for 1 mg/mL L-cysteine concentration were taken from Table 1. All values are presented as mean ± SD ($n = 3$).

(82% ± 5%), the smallest average particle size (228 ± 3 nm), a low polydispersity index, and the highest absolute zeta potential values were observed. As the experiment demonstrated, HSA nanoparticles prepared at the biopolymer concentration of 40 mg/mL were relatively stable over time. Analysis of samples within a week showed no particle aggregation or structure degradation. When the drug is included, this concentration remains optimal, taking into account all parameters (particle diameter 302 ± 6 nm, PDI 0.046 ± 0.018, yield 64% ± 9%) and characteristics (encapsulation efficiency 85% ± 7%).

3.1.6 | Effect of Isoniazid Concentration

The antituberculosis drug INH was loaded into albumin nanoparticles as a model biologically active substance. Drug loading was carried out by incorporating isoniazid during the preparation of HSA nanoparticles, followed by a 2 h incubation period [22–24]. The drug concentration ranged from 2 to 8 mg/mL. The results are presented in Table 6.

The results presented in the table indicate a significant effect of drug concentration on the characteristics of the system. The encapsulation efficiency and NPs yield decreased with increasing isoniazid concentration, whereas drug loading showed a corresponding increase. A high drug content in the polymer was achieved (73% ± 5%), although the nanoparticles yield remained relatively low (31% ± 3%). Particle diameter and polydispersity index were within optimal ranges at 230 ± 6 nm and 0.160 ± 0.045, respectively. Considering the requirement for therapeutic efficacy, a drug concentration of 8 mg/mL was identified as the most suitable.

For further application of the produced albumin nanoparticles both in research and practical context, it is important to ensure their stability over a defined period. Therefore, the stability of the nanoparticles prepared under optimized conditions (C_{HSA} = 40 mg/mL, $C_{L\text{-cysteine}}$ = 5 mg/mL, C_{urea} 4 mol/L, pH 6, in case with drug C_{INH} = 8 mg/mL) was evaluated for 8 days at room temperature (25°C). The measurement of HSA NPs demonstrated (Figure S6) an average particle size ranging from 304 ± 4 to 392 ± 5 nm, with slight variations. During the same observation period, HSA-INH NPs maintained consistent size measurements between 321 ± 2 and 366 ± 3 nm. At all measured time points, HSA nanoparticles retained a narrow size distribution, with PDI values below 0.2, which indicates a stable nanoparticle dispersion without signs of aggregation. These results confirm the stability of the albumin-based nanoparticle

TABLE 5 | Characteristics of nanoparticles and production efficiency prepared using different HSA concentrations.

		Characteristics			Production efficiency		
Nanoparticles	HSA concentration (mg/mL)	Size (nm)	PDI	Zeta potential (mV)	Encapsulation efficiency (%)	Drug loading (%)	NPs yield (%)
HSA	10	238 ± 7	0.165 ± 0.134	−21 ± 4	—	—	68 ± 3
	20	244 ± 7	0.317 ± 0.021	−14 ± 3	—	—	69 ± 5
	40	228 ± 3	0.316 ± 0.019	−35 ± 6	—	—	82 ± 5
	80	786 ± 7	0.315 ± 0.061	−21 ± 12	—	—	60 ± 5
HSA-INH	10	315 ± 3	0.029 ± 0.010	−22 ± 2	75 ± 7	17 ± 3	74 ± 9
	20	394 ± 9	0.232 ± 0.067	−21 ± 3	85 ± 2	15 ± 2	56 ± 5
	40	302 ± 6	0.046 ± 0.018	−34 ± 4	85 ± 7	7 ± 3	64 ± 9
	80	209 ± 7	0.411 ± 0.030	−30 ± 4	85 ± 4	4 ± 3	53 ± 5

Note: All conditions, except HSA concentration, were consistent with standard parameters. Data corresponding to the 20 mg/mL HSA concentration were taken from Table 1. All values are presented as mean ± SD (n = 3).

TABLE 6 | Characteristics of nanoparticles and production efficiency using different isoniazid concentrations.

		Characteristics			Production efficiency		
Nano-particles	INH concentration (mg/mL)	Size (nm)	PDI	Zeta potential (mV)	Encapsulation efficiency (%)	Drug loading (%)	NPs yield (%)
HSA-INH	2	394 ± 9	0.232 ± 0.067	−21 ± 3	85 ± 2	15 ± 2	56 ± 5
	4	238 ± 8	0.317 ± 0.025	−28 ± 2	80 ± 5	19 ± 3	72 ± 5
	6	262 ± 7	0.193 ± 0.049	−29 ± 4	82 ± 4	43 ± 5	44 ± 5
	8	230 ± 6	0.160 ± 0.045	−24 ± 3	78 ± 4	73 ± 5	31 ± 3

Note: All conditions, except INH concentration, were consistent with standard parameters. All values are presented as mean ± SD (n = 3).

system, supporting its potential as a promising carrier for further development in controlled drug delivery.

3.2 | Physicochemical Characteristics of HSA-NP Loaded With Isoniazid

Nanoparticles produced under optimal conditions were used to investigate their physicochemical parameters. Morphological analysis of HSA NPs and HSA-INH NPs samples was conducted using SEM, with the resulting images presented in Figure 4. ImageJ software was used to analyze the images, revealing average particle sizes of 226 ± 7 and 220 ± 5 nm for HSA and HSA-INH nanoparticles, respectively. Both types of nanoparticles exhibited a spherical morphology.

TGA (a) and DSC (b) thermograms of isoniazid (INH), drug-free HSA nanoparticles, and HSA nanoparticles loaded with INH are shown in Figure 5. The results showed a slower degradation of albumin nanoparticles loaded with isoniazid, indicating its improved stability compared with drug-free albumin nanoparticles. TGA profile shows the temperature stability and degradation behavior of HSA-INH nanoparticles as a function of increasing temperature (Figure 5a). The onset of degradation is observed at ~240°C. A sharp weight loss occurs beyond 300°C, likely due to the release of small volatile compounds such as carbon dioxide and ammonia [48]. A characteristic endothermic peak for INH appears at 177.2°C in the DSC thermogram (Figure 6b), corresponding to its melting point and indicating its crystalline nature. Additionally, an exothermic peak is observed at 361.8°C, accompanied by a weight loss of up to 74% within the 250°C–370°C range (Figure 5a), which is attributed to drug decomposition. Notably, the endothermic peak associated with crystalline isoniazid is absent in the thermogram of HSA-INH nanoparticles (Figure 6b), suggesting the drug is present in an amorphous form or is molecularly dispersed within the nanoparticle matrix [49].

FTIR spectra of isoniazid, drug-free HSA nanoparticles, and HSA-INH nanoparticles were recorded (Figure 6). The spectra show characteristic bands for albumin, including a broad band at

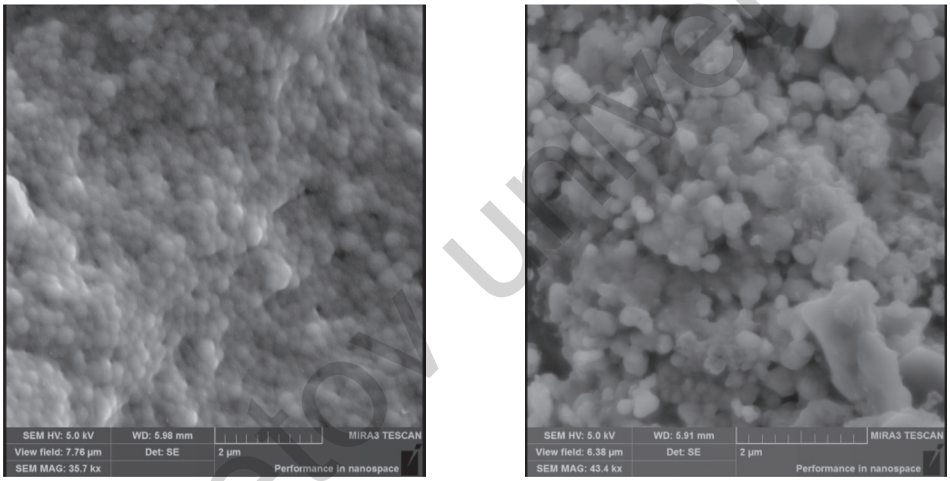

FIGURE 4 | SEM images of HSA-NPs (a) and HSA-INH NPs (b).

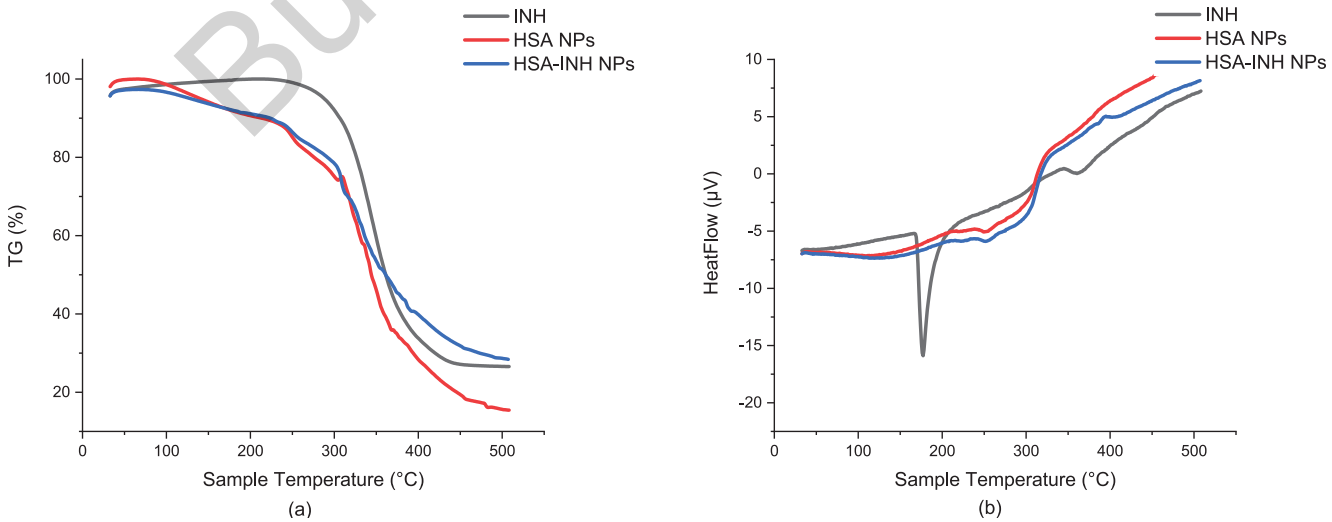

FIGURE 5 | TGA (a) and DSC (b) thermograms for isoniazid, HSA nanoparticles, and HSA-INH nanoparticles.

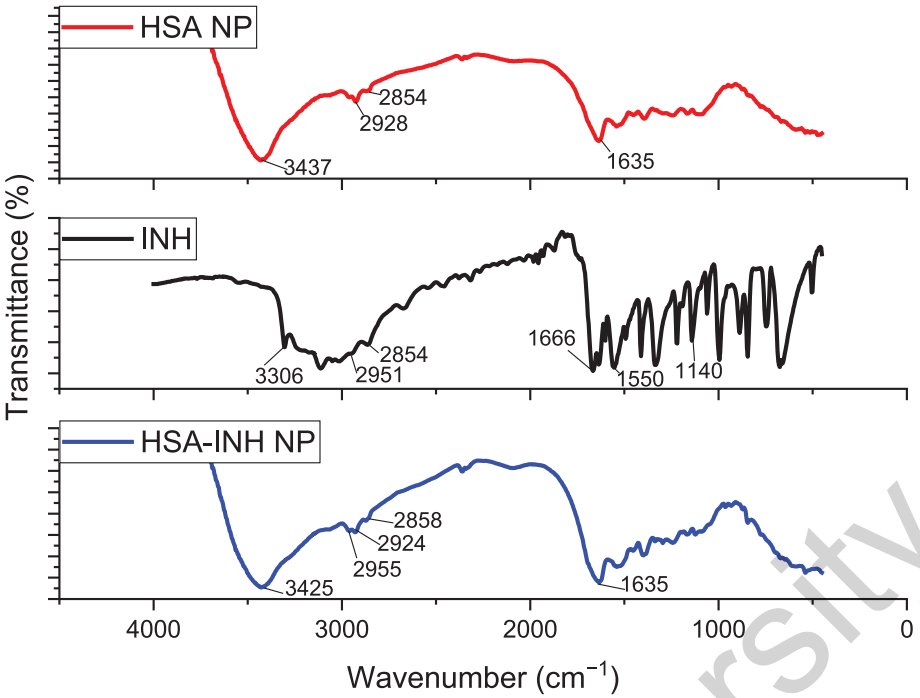

FIGURE 6 | FT-IR spectra of isoniazid, drug-free HSA nanoparticles, and HSA nanoparticles loaded with isoniazid.

3437 cm^{-1} (amide A, NH– stretching), a sharp peak at 2928 cm^{-1} (amide B, associated with free ions), and amide II at 1535 cm^{-1}, corresponding to –CN stretching and –NH bending vibrations. The amide I peak at 1635 cm^{-1} is attributed to –C–O stretching, while $-CH_2$ groups appear at 1396 cm^{-1}, and amide III at ~1245 cm^{-1} is associated with –C–N stretching and N–H bending vibrations [50]. The FTIR spectrum of isoniazid (Figure 6) shows characteristic absorption bands at 3310 cm^{-1} ($-NH_2$ stretching), 1666 cm^{-1} (–C=O conjugated with the pyridine ring), 1550 cm^{-1} (–CN stretching), and 1140 cm^{-1} (–N–N amide group). The spectrum of HSA-INH-NPs shows characteristic peaks for both the protein and isoniazid, indicating the absence of chemical bonding between the drug and the nanoparticle matrix. Previous molecular dynamics and spectroscopic studies [27, 51] have shown that electrostatic interactions and hydrogen bonding are the primary forces governing the interaction between drugs and albumin.

The release of isoniazid from HSA nanoparticles was studied using three samples prepared with initial drug concentrations of 4, 6, and 8 mg/mL (Figure 7).

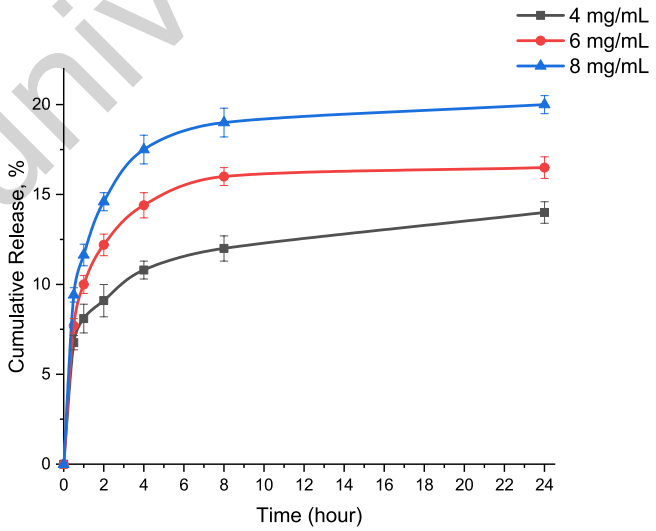

FIGURE 7 | Isoniazid release from albumin nanoparticles prepared using 4, 6, and 8 mg/mL of the drug in the initial mixture.

HSA-INH nanoparticles prepared under optimized conditions were dispersed in 7 mL of phosphate buffered saline (PBS; pH = 7.4) at 200 rpm and 37°C. The amount of isoniazid released was determined for 24 h. Approximately 20% of the drug was released within 24 h from the HSA-INH nanoparticles prepared at isoniazid concentration 8 mg/mL. The burst release of the drug at the beginning of the process can be explained by the release of weakly bound isoniazid, mainly from the nanoparticles surface. Further release occurs, most likely, due to the diffusion of the drug molecules from the inner part of the nanoparticles as a result of their partial degradation [52]. This enables the development of an HSA-INH nanoparticle-based drug delivery system for sustained release of active ingredients against mycobacteria.

Table 7 presents the results of a comparative analysis of mathematical models used to describe the release kinetics from albumin nanoparticles at isoniazid concentrations of 4, 6, and 8 mg/mL. Two models were evaluated: the Korsmeyer–Peppas model ($M_t/M_\infty = kt^n$), which characterizes diffusion-controlled release, particularly in the initial phase; and the Peppas–Sahlin model ($M_t/M_\infty = kt^m + k_2t^{2m}$), which accounts for both Fickian diffusion and relaxation of the polymer matrix [53–55].

Based on the coefficient of determination (R^2), the Peppas–Sahlin model provided the best fit to the experimental data ($R^2 > 0.99$), confirming its suitability for describing a combined release mechanism involving both diffusion and polymer relaxation. The Korsmeyer–Peppas model also yielded good results

($R^2 = 0.88–0.98$), suggesting that diffusion plays a predominant role. Overall, the analysis indicates that the Peppas–Sahlin model is the most appropriate for describing the kinetics of isoniazid release from the albumin-based polymeric matrix.

3.3 | In Vitro Assessment of the Inhibitory Activity of Isoniazid-Loaded HSA Nanoparticles on MTB

To evaluate whether isoniazid-loaded HSA nanoparticles retain their anti-tuberculosis activity, the drug-loaded nanoparticles were tested against the wild strain of *Mycobacterium tuberculosis* H37Rv. The samples were incubated on Levenstein–Jensen medium for 4 weeks, and the results were subsequently recorded. Figure 8a presents a histogram of the number of colony forming units (CFU/10^7 cells) of *Mycobacterium tuberculosis* following treatment with different formulations: control (no nanoparticles added), drug-free HSA nanoparticles (without isoniazid), and HSA-INH nanoparticles with isoniazid concentrations of 5, 25, and 50 mg/mL.

As shown, the addition of INH-loaded nanoparticles resulted in a statistically significant reduction in bacterial growth compared with both the control and drug-free groups, with the inhibitory effect increasing in a concentration-dependent manner. The reduction in CFU counts at 25 and 50 mg/mL was particularly pronounced, confirming the high efficacy of nanoparticle-loaded isoniazid. The minimum effective concentration of isoniazid in HSA-INH nanoparticles required to achieve substantial suppression of MTB growth was determined to be 25 mg/mL. Photographic documentation of the experimental samples obtained during the microbiological study further supports these findings (Figure S7).

Figure 8b presents microscopic images of Ziehl–Nielsen-stained smears, illustrating differences in MTB growth among the treated groups. High mycobacterial density is observed in both the control and drug-free nanoparticle groups, whereas a noticeable reduction in bacterial presence is evident with INH-loaded nanoparticles at a concentration of 5 mg/mL. These data confirm that loading of INH in albumin nanoparticles

TABLE 7 | Model parameters describing isoniazid release from HSA-INH nanoparticles.

Concentration of isoniazid in HSA-INH nanoparticles	Korsmeyer–Peppas			Peppas–Sahlin		
	k	n	R^2	k_1	m	R^2
4 mg/mL	8.08	0.18	0.986	9.52	0.28	0.998
6 mg/mL	10.36	0.17	0.876	11.99	0.38	0.997
8 mg/mL	12.38	0.17	0.885	14.33	0.38	0.995

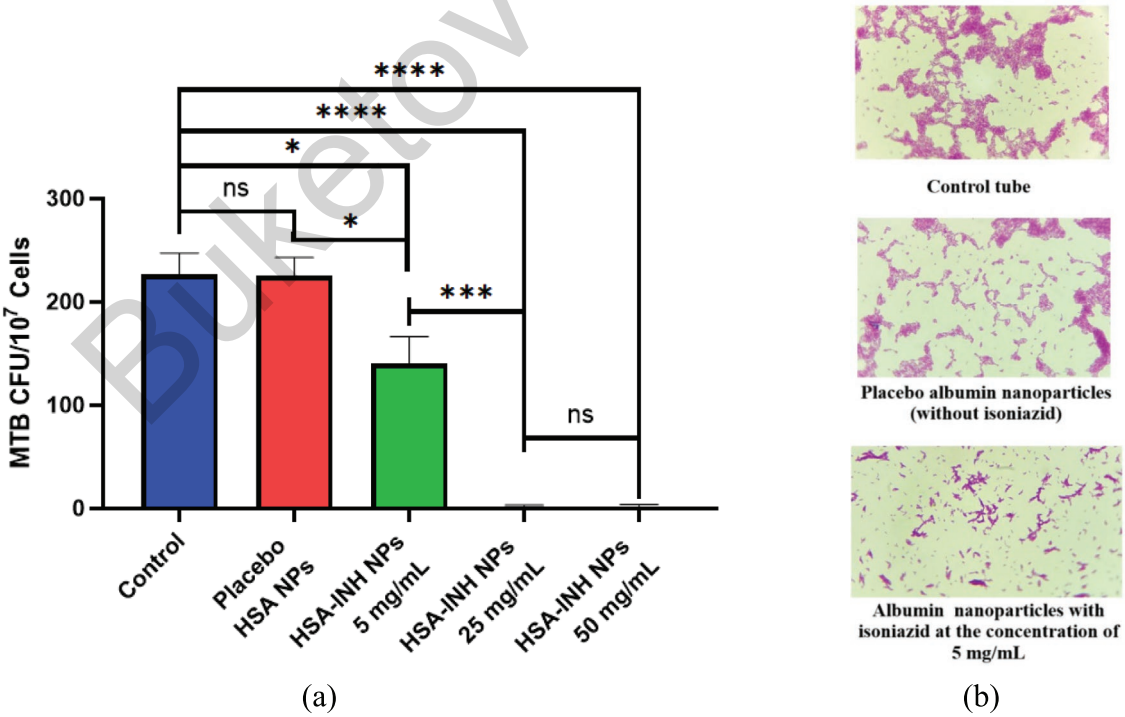

FIGURE 8 | Results of microbiological activity test of the samples on the growth of *Mycobacterium tuberculosis* H37Rv on Levenstein-Jensen nutrient-dense medium. "*," "**," and "****" indicate $p < 0.01$, $p < 0.005$ and $p < 0.0001$, respectively, ns—denotes no significant difference. Data are presented as mean ± standard error of the mean ($n = 3$). (b) Microphotographs of *Mycobacterium tuberculosis* H37Rv growth on the samples, stained using the Ziehl–Neelsen method.

enhances its antimycobacterial activity and may contribute to the improved therapeutic outcomes in the treatment of tuberculosis.

4 | Conclusion

Desolvation of HSA using ethanol followed by stabilization of the dispersion with L-cysteine represents a promising approach for the preparation of polymer nanoparticles for antituberculosis drug delivery. The physicochemical characteristics of the resulting biopolymer nanoparticles during drug loading are influenced by the concentrations of HSA, L-cysteine, urea, and INH in the formulation. Additionally, the pH of the medium and the concentration of these components determine both the yield and stability of the nanoparticles, as well as their drug loading capacity. The optimal pH range for this system lies between pH 5 and 7, with the most stable NPs obtained at pH 6, likely due to pH-induced conformational changes in the protein structure.

Optimal synthesis conditions were achieved with the inclusion of urea, which functions as a mild chaotropic agent. Urea interacts reversibly with proteins, disrupting intermolecular hydrogen bonds and facilitating partial denaturation. Unlike heat-induced denaturation, urea-induced protein unfolding follows a stepwise mechanism involving reversible transitions between unfolded and refolded states.

L-cysteine contributes to HSA nanoparticles stabilization through the formation of intermolecular disulfide bonds via the thiol-disulfide exchange, thereby enhancing structural integrity. The observed dependence of nanoparticle stability on L-cysteine concentration supports the occurrence of post-translational modifications of HSA under these conditions.

HSA nanoparticles stabilized in this manner demonstrated a high loading capacity, with more than 70% encapsulation efficiency of isoniazid. In vitro studies of HSA-INH nanoparticles confirmed their potential for sustained drug release and effective suppression of *Mycobacterium tuberculosis*. Specifically, treatment with HSA-INH nanoparticles resulted in complete and significant inhibition of the wild-type H37Rv strain, supporting their suitability as a controlled drug delivery system for tuberculosis therapy.

Author Contributions

Aldana Galiyeva: writing – original draft, methodology, investigation, data curation, funding acquisition. **Yerkeblan Tazhbayev:** writing – review and editing, supervision, funding acquisition, conceptualization. **Tolkyn Zhumagaliyeva:** validation, formal analysis. **Bakhytgul Karimova:** investigation. **Nurlan Tabriz:** investigation. **Vitaliy V. Khutoryanskiy:** writing – review and editing.

Acknowledgments

During the preparation of this work, the authors used ChatGPT in order to refine the language of the manuscript. After using this tool/service, the authors reviewed and edited the content as needed and took full responsibility for the content of the publication.

Conflicts of Interest

The authors declare no conflicts of interest.

Data Availability Statement

The data that supports the findings of this study are available in the Supporting Information S1 of this article.

References

1. World Health Organization, *Global Tuberculosis Report 2024* (World Health Organization, 2024), https://www.who.int/news/item/29-10-2024-tuberculosis-resurges-as-top-infectious-disease-killer.

2. M. Mazlan, M. M. Tazizi, R. Ahmad, et al., "Antituberculosis Targeted Drug Delivery as a Potential Future Treatment Approach," *Antibiotics* 10, no. 8 (2021): 908, https://doi.org/10.3390/antibiotics10080908.

3. L. Lawson, M. Muc, O. Oladimeji, et al., "Tuberculosis and Diabetes in Nigerian Patients With and Without HIV," *International Journal of Infectious Diseases* 61 (2017): 121–125, https://doi.org/10.1016/j.ijid.2017.06.014.

4. K. Ronacher, S. A. Joosten, R. van Crevel, H. M. Dockrell, G. Walzl, and T. H. Ottenhoff, "Acquired Immunodeficiencies and Tuberculosis: Focus on HIV/AIDS and Diabetes Mellitus," *Immunological Reviews* 264, no. 1 (2015): 121–137, https://doi.org/10.1111/imr.12257.

5. A. Allué-Guardia, J. I. García, and J. B. Torrelles, "Evolution of Drug-Resistant *Mycobacterium tuberculosis* Strains and Their Adaptation to the Human Lung Environment," *Frontiers in Microbiology* 12 (2021): 1–21, https://doi.org/10.3389/fmicb.2021.612675.

6. L. B. Kim and A. N. Putyatina, "Mechanism of Lungs Fibrosis in Mycobacterial Infection," *Exploration of Medicine* 4 (2023): 956–976, https://doi.org/10.37349/emed.2023.00187.

7. Centers for Disease Control and Prevention, *Treatment for TB Disease* (CDC, 2016), https://www.cdc.gov/tb/topic/treatment/tbdisease.htm.

8. T. Gumbo, A. Louie, W. Liu, et al., "Isoniazid Bactericidal Activity and Resistance Emergence: Integrating Pharmacodynamics and Pharmacogenomics to Predict Efficacy in Different Ethnic Populations," *Antimicrobial Agents and Chemotherapy* 51, no. 7 (2007): 2329–2336, https://doi.org/10.1128/aac.00185-07.

9. L. Jena, P. Waghmare, S. Kashikar, S. Kumar, and B. C. Harinath, "Computational Approach to Understanding the Mechanism of Action of Isoniazid, an Anti-TB Drug," *International Journal of Mycobacteriology* 3, no. 4 (2014): 276–282, https://doi.org/10.1016/j.ijmyco.2014.08.003.

10. T. Bourguignon, J. A. Godinez-Leon, and R. Gref, "Nanosized Drug Delivery Systems to Fight Tuberculosis," *Pharmaceutics* 15, no. 2 (2023): 393, https://doi.org/10.3390/pharmaceutics15020393.

11. K. Dua, V. K. Rapalli, S. D. Shukla, et al., "Multi-Drug Resistant *Mycobacterium tuberculosis* & Oxidative Stress Complexity: Emerging Need for Novel Drug Delivery Approaches," *Biomedicine & Pharmacotherapy* 107 (2018): 1218–1229, https://doi.org/10.1016/j.biopha.2018.08.101.

12. E. Kianfar, "Protein Nanoparticles in Drug Delivery: Animal Protein, Plant Proteins and Protein Cages, Albumin Nanoparticles," *Journal of Nanobiotechnology* 19, no. 1 (2021): 159, https://doi.org/10.1186/s12951-021-00896-3.

13. O. Opriș, C. Mormile, I. Lung, A. Stegarescu, M.-L. Soran, and A. Soran, "An Overview of Biopolymers for Drug Delivery Applications," *Applied Sciences* 14, no. 4 (2024): 1383, https://doi.org/10.3390/app14041383.

14. C. Weber, C. Coester, J. Kreuter, and K. Langer, "Desolvation Process and Surface Characterisation of Protein Nanoparticles," *International*

Journal of Pharmaceutics 194 (2000): 91–102, https://doi.org/10.1016/s0378-5173(99)00370-1.

15. K. Langer, S. Balthasar, V. Vogel, N. Dinauer, H. von Briesen, and D. Schubert, "Optimization of the Preparation Process for Human Serum Albumin (HSA) Nanoparticles," *International Journal of Pharmaceutics* 257 (2003): 169–180, https://doi.org/10.1016/s0378-5173(03)00134-0.

16. B. von Storp, A. Engel, A. Boeker, M. Ploeger, and K. Langer, "Albumin Nanoparticles With Predictable Size by Desolvation Procedure," *Journal of Microencapsulation* 29 (2011): 138–146, https://doi.org/10.3109/02652048.2011.635218.

17. K. Kimura, K. Yamasaki, H. Nakamura, M. Haratake, K. Taguchi, and M. Otagiri, "Preparation and In Vitro Analysis of Human Serum Albumin Nanoparticles Loaded With Anthracycline Derivatives," *Chemical & Pharmaceutical Bulletin* 66, no. 4 (2018): 382–390, https://doi.org/10.1248/cpb.c17-00838.

18. Agency for Toxic Substances and Disease Registry, *Toxicological Profile for Glutaraldehyde* (Agency for Toxic Substances and Disease Registry, 2017), https://www.ncbi.nlm.nih.gov/books/NBK591671/.

19. P. Umashankar, T. Kumari, and P. Mohanan, "Glutaraldehyde Treatment Elicits Toxic Response Compared to Decellularization in Bovine Pericardium," *Toxicology International* 19, no. 1 (2012): 51–58, https://doi.org/10.4103/0971-6580.94513.

20. E. Argitekin, O. Erez, G. Cakan-Akdogan, and Y. Akdogan, "Periodate-Mediated Cross-Linking for the Preparation of Catechol Conjugated Albumin Nanoparticles Used for In Vitro Drug Delivery," *ACS Applied Bio Materials* 8, no. 3 (2025): 2182–2193, https://doi.org/10.1021/acsabm.4c01737.

21. D. Hense and O. I. Strube, "Glutaraldehyde Cross-Linking of Salt-Induced Fibrinogen Hydrogels," *ACS Biomaterials Science & Engineering* 10, no. 11 (2024): 6927–6937, https://doi.org/10.1021/acsbiomaterials.4c01412.

22. Y. Tazhbayev, O. Mukashev, M. Burkeev, and J. Kreuter, "Hydroxyurea-Loaded Albumin Nanoparticles: Preparation, Characterization, and In Vitro Studies," *Pharmaceutics* 11 (2019): 410, https://doi.org/10.3390/pharmaceutics11080410.

23. Y. Tazhbayev, O. Mukashev, M. Burkeyev, and V. I. Lozinsky, "Synthesis and Comparative Study of Nanoparticles Derived From Bovine and Human Serum Albumins," *Polymers* 12 (2020): 1301, https://doi.org/10.3390/polym12061301.

24. Y. Tazhbayev, A. Galiyeva, T. Zhumagaliyeva, M. Burkeyev, and B. Karimova, "Isoniazid—Loaded Albumin Nanoparticles: Taguchi Optimization Method," *Polymers* 13 (2021): 3808, https://doi.org/10.3390/polym13213808.

25. E. O. Shatabayeva, D. B. Kaldybekov, L. Ulmanova, et al., "Enhancing Mucoadhesive Properties of Gelatin Through Chemical Modification With Unsaturated Anhydrides," *Biomacromolecules* 25, no. 3 (2024): 1612–1628, https://doi.org/10.1021/acs.biomac.3c01183.

26. E. G. Dzodanu, J. Afrifa, D. O. Acheampong, and I. Dadzie, "Diagnostic Yield of Fluorescence and Ziehl-Neelsen Staining Techniques in the Diagnosis of Pulmonary Tuberculosis: A Comparative Study in a District Health Facility," *Tuberculosis Research and Treatment* 2019 (2019): 1–6, https://doi.org/10.1155/2019/4091937.

27. S. Vallie and S. Naidoo, "Identification of the Binding Interaction of Anti-TB Drugs With Human Serum Albumin: A Computational Molecular Docking, Fluorescence and Absorption Spectroscopy Study," *International Journal of Pharmaceutical Quality Assurance* 11, no. 1 (2020): 1–14, https://doi.org/10.25258/ijpqa.11.1.00.

28. I. A. Rodionov, N. V. Grinberg, T. V. Burova, V. Y. Grinberg, and V. I. Lozinsky, "Cryostructuring of Polymer Systems. Proteinaceous Wide-Pore Cryogels Generated by the Action of Denaturant/Reductant Mixtures on Bovine Serum Albumin in Moderately-Frozen Aqueous Media," *Soft Matter* 11 (2015): 4921–4931, https://doi.org/10.1039/C4SM02814G.

29. N. Lomis, S. Westfall, L. Farahdel, M. Malhotra, D. Shum-Tim, and S. Prakash, "Human Serum Albumin Nanoparticles for Use in Cancer Drug Delivery: Process Optimization and In Vitro Characterization," *Nanomaterials* 6 (2016): 116, https://doi.org/10.3390/nano6060116.

30. M. Z. Burkeev, J. Kreuter, Y. M. Tazhbayev, L. Z. Zhaparova, and T. S. Zhumagalieva, "Preparation, Characterization and Investigation of In Vitro Release of Anti-Tuberculosis Drug p-Amino Salicylic Acid Based on Human Serum Albumin," *Bulletin of the Karaganda University* 87 (2017): 38–44, https://doi.org/10.31489/2017ch3/38-44.

31. A. Costa, M. Pinheiro, J. Magalhães, et al., "The Formulation of Nanomedicines for Treating Tuberculosis," *Advanced Drug Delivery Reviews* 102 (2016): 102–115, https://doi.org/10.1016/j.addr.2016.04.012.

32. P. Avdeev, V. Ignatenko, Y. Kornoushenko, and L. Evtuhova, "Effect of Different Concentrations of Urea and pH on the Fluorescence Parameters of Bovine Serum Albumin," *Health and Ecology Issues* 1 (2011): 106–110, https://doi.org/10.51523/2708-6011.2011-8-1-20.

33. N. G. Zhdanova, "Relation of Photophysical Parameters of Tyrosine Residues in Serum Albumin to Changes in Protein Structure Under the Influence of Ligands and Denaturation," Candidate's Thesis, Moscow (2016), http://www.sinp.msu.ru/ru/dissertation/25235.

34. A. Srivastava and A. Prajapati, "Albumin and Functionalized Albumin Nanoparticles: Production Strategies, Characterization, and Target Indications," *Asian Biomedicine* 14, no. 6 (2020): 217–242, https://doi.org/10.1515/abm-2020-0032.

35. S. Hong, D. W. Choi, H. N. Kim, C. G. Park, W. Lee, and H. H. Park, "Protein-Based Nanoparticles as Drug Delivery Systems," *Pharmaceutics* 12, no. 7 (2020): 604, https://doi.org/10.3390/pharmaceutics12070604.

36. M. Dockal, D. C. Carter, and F. Rüker, "Conformational Transitions of the Three Recombinant Domains of Human Serum Albumin Depending on pH," *Journal of Biological Chemistry* 275 (2000): 3042–3050, https://doi.org/10.1074/jbc.275.5.3042.

37. V. I. Lozinsky and O. Okay, "Basic Principles of Cryotropic Gelation," *Advances in Polymer Science* 263 (2014): 49–101, https://doi.org/10.1007/978-3-319-05846-7_2.

38. M. Tarhini, A. Pizzoccaro, I. Benlyamani, et al., "Human Serum Albumin Nanoparticles as Nanovector Carriers for Proteins: Application to the Antibacterial Proteins 'Neutrophil Elastase' and 'Secretory Leukocyte Protease Inhibitor'," *International Journal of Pharmaceutics* 579 (2020): 119150, https://doi.org/10.1016/j.ijpharm.2020.119150.

39. M. Poudyal, K. Patel, L. Gadhe, et al., "Intermolecular Interactions Underlie Protein/Peptide Phase Separation Irrespective of Sequence and Structure at Crowded Milieu," *Nature Communications* 14, no. 1 (2023): 1–21, https://doi.org/10.1038/s41467-023-41864-9.

40. K. Grigoryan, "Denaturation of Human Serum Albumin at the Presence of Urea–Dimethylsulfoxide Complexes," *Scientific Notes of the Yerevan State University. Chemistry and Biology* 2 (2010): 3–6, https://doi.org/10.46991/PYSU:B/2010.44.2.003.

41. D. R. Canchi, D. Paschek, and A. E. García, "Equilibrium Study of Protein Denaturation by Urea," *Journal of the American Chemical Society* 132, no. 7 (2010): 2338–2344, https://doi.org/10.1021/ja909348c.

42. D. Li, D. Hong, H. Guo, J. Chen, and B. Ji, "Probing the Influences of Urea on the Interaction of Sinomenine With Human Serum Albumin by Steady-State Fluorescence," *Journal of Photochemistry and Photobiology B* 117 (2012): 126–131, https://doi.org/10.1016/j.jphotobiol.2012.09.007.

43. N. Zhdanova, E. Shirshin, E. Maksimov, I. Panchishin, A. M. Saletsky, and V. V. Fadeev, "Tyrosine Fluorescence Probing of the Surfactant-Induced Conformational Changes of Albumin," *Photochemical & Photobiological Sciences* 14, no. 5 (2015): 897–908, https://doi.org/10.1039/c4pp00432a.

44. N. G. Zhdanova, E. G. Maksimov, A. M. Arutyunyan, V. V. Fadeev, and E. A. Shirshin, "Tyrosine Fluorescence Probing of Conformational

Changes in Tryptophan-Lacking Domain of Albumins," *Spectrochimica Acta. Part A, Molecular and Biomolecular Spectroscopy* 174 (2017): 223–229, https://doi.org/10.1016/j.saa.2016.11.038.

45. L. B. Sagle, Y. Zhang, V. A. Litosh, X. Chen, Y. Cho, and P. S. Cremer, "Investigating the Hydrogen-Bonding Model of Urea Denaturation," *Journal of the American Chemical Society* 131, no. 26 (2009): 9304–9310.

46. R. Kumaran and P. Ramamurthy, "Denaturation Mechanism of BSA by Urea Derivatives: Evidence for Hydrogen-Bonding Mode From Fluorescence Tools," *Journal of Fluorescence* 21, no. 4 (2011): 1499–1508, https://doi.org/10.1007/s10895-011-0836-0.

47. S. Muzammil, Y. Kumar, and S. Tayyab, "Anion-Induced Stabilization of Human Serum Albumin Prevents the Formation of Intermediate During Urea Denaturation," *Proteins* 40, no. 1 (2000): 29–38, https://doi.org/10.1002/(sici)1097-0134(20000701)40:1<29::aid-prot50>3.0.co;2-p.

48. P. Singh, H. Singh, V. Castro-Aceituno, S. Ahn, Y. J. Kim, and D. C. Yang, "Bovine Serum Albumin as a Nanocarrier for the Efficient Delivery of Ginsenoside Compound K: Preparation, Physicochemical Characterizations and In Vitro Biological Studies," *RSC Advances* 7, no. 25 (2017): 15397–15407, https://doi.org/10.1039/c6ra25264h.

49. W. Wang, Y. Lei, H. Sui, et al., "Fabrication and Evaluation of Nanoparticle-Assembled BSA Microparticles for Enhanced Liver Delivery of Glycyrrhetinic Acid," *Artificial Cells, Nanomedicine, and Biotechnology* 45, no. 4 (2017): 740–747, https://doi.org/10.1080/21691401.2016.1193024.

50. A. Galiyeva, A. Daribay, N. Tabriz, and Y. Tazhbayev, "Production of Polylactide Nanoparticles Loaded With Isoniazid and Vitamin C: A Promising Candidate for the Treatment of Resistant Forms of Tuberculosis," *Journal of Polymer Science* (Early View), https://doi.org/10.1002/pol.20240375.

51. J. Yu, Y. Chen, L. Xiong, X. Zhang, and Y. Zheng, "Conductance Changes in Bovine Serum Albumin Caused by Drug-Binding Triggered Structural Transitions," *Materials* 12, no. 7 (2019): 1022, https://doi.org/10.3390/ma12071022.

52. A. Galiyeva, A. Daribay, T. Zhumagaliyeva, L. Zhaparova, D. Sadyrbekov, and Y. Tazhbayev, "Human Serum Albumin Nanoparticles: Synthesis, Optimization and Immobilization With Antituberculosis Drugs," *Polymers* 15 (2023): 2774, https://doi.org/10.3390/polym15132774.

53. J. Zhang, M. Fu, M. Zhang, L. Xu, and Y. Gao, "Synthesis of Oxidized Glycerol Monooleate-Chitosan Polymer and Its Hydrogel Formation for Sustained Release of Trimetazidine Hydrochloride," *International Journal of Pharmaceutics* 465, no. 1–2 (2014): 32–41, https://doi.org/10.1016/j.ijpharm.2014.02.001.

54. M. L. Bruschi, *Strategies to Modify the Drug Release From Pharmaceutical Systems* (Elsevier, 2015), 63–86.

55. E. Damasceno Junior, R. M. Barbosa, R. C. D. da Silva, et al., "Montmorillonite–Rifampicin Nanohybrid for pH-Responsive Release of the Tuberculostatic," *Pharmaceutics* 15, no. 2 (2023): 512, https://doi.org/10.3390/pharmaceutics15020512.

Supporting Information

Additional supporting information can be found online in the Supporting Information section.